Hydrothermal Syntheses and Crystal Structures of Two Oxovanadium−Organodiphosphonate Phases: $[H_2N(C_2H_4)_2NH_2][(VO)_2(O_3PCH_2CH_2CH_2PO_3H)_2]$, a "Stair-Step" Structure Incorporating an Organic Cationic Template, and $[(VO)(H_2O)\{O_3PCH_2NH(C_2H_4)_2NHCH_2PO_3\}]$, a Layered Structure "Pillared" by a Piperazinium-Tethered Diphosphonate

Victoria Soghomonian,[1a] Roberto Diaz,[1c] Robert C. Haushalter,*[,1b] Charles J. O'Connor,[1d] and Jon Zubieta*[,1a]

Department of Chemistry, Syracuse University, Syracuse, New York 13244, NEC Research Institute, 4 Independence Way, Princeton, New Jersey 08540, and Department of Chemistry, University of New Orleans, New Orleans, Louisiana 70148

Received February 3, 1995[⊗]

Two new members of the oxovanadium−organodiphosphonate system, $V-O-R(PO_3)_2^{4-}$, have been synthesized by hydrothermal methods and structurally characterized. The reaction of VCl_4, propylenediphosphonic acid, piperazine, and H_2O in the mole ratio 1:1.5:3:945 at 200 °C and 96 h yields $[H_2N(C_2H_4)_2NH_2][(VO)_2(O_3PCH_2CH_2CH_2PO_3H)_2]$ (**1**), as green rodlike crystals. The structure consists of ribbons of corner-sharing vanadium square pyramids and phosphorus tetrahedra interconnected by the diphosphonate organic backbone into a stair-step structural motif. The reaction of VCl_4, *N,N'*-piperazinebis(methylenephosphonic acid), and H_2O in the mole ratio 1:0.8:570 at 125 °C for 134 h yields $[(VO)(H_2O)\{O_3PCH_2NH(C_2H_4)_2NHCH_2PO_3\}]$ (**2**), as light aqua green crystals of cubic habit. The structure of **2** consists of inorganic V/P/O layers linked through the organodiphosphonate backbone into an array of alternating inorganic and organic layers. In contrast to those in **1**, the vanadium sites are six-coordinate and the V/P/O layer structure is a defected form of the V−P−O ribbon of **1** with alternate vanadium sites vacant. Compound **1** exhibits magnetic properties consistent with antiferromagnetic coupling of the V(IV) sites, with $J/k = -10.3$ K as an estimate of the strength of the exchange. Crystal data: $C_{10}H_{26}N_2O_{14}P_4V_2$ (**1**), triclinic $P\bar{1}$, $a = 6.244(1)$ Å, $b = 8.687(2)$ Å, $c = 11.156(2)$ Å, $\alpha = 88.92(3)°$, $\beta = 74.63(3)°$, $\gamma = 74.32(3)°$, $V = 560.8(3)$ Å^3, $Z = 1$, $D_{calc} = 1.842$ g cm^{-3}, with structure solution and refinement based on 1663 reflections converging at $R = 0.0662$; $C_6H_{12}N_2O_8P_2V$ (**2**), monoclinic $P2_1/c$, $a = 7.999(2)$ Å, $b = 8.009(2)$ Å, $c = 9.201(2)$ Å, $\beta = 100.24(3)°$, $V = 580.1(3)$ Å^3, $Z = 2$, $D_{calc} = 2.021$ g cm^{-3}, 1453 reflections, $R = 0.0593$.

The expansion of research activity in the chemistry of the metal organophosphonates[2−4] reflects their interesting fundamental coordination chemistry and their practical applications as catalysts, hosts in intercalation compounds, sorbents, and ion-exchangers.[5−15] Furthermore, the self-assembly of transition metal phosphonates on surfaces[16,17] provides an attractive method for constructing thermally and solvolytically stable films of controlled thickness having spatically defined molecular components and possessing potentially useful optical, nonlinear optical, or electronic properties.[18−20]

The vanadyl organophosphonates are represented by the prototypical materials $[VO(H_2O)(PhPO_3)]$[21−23] and $[(VO)_2(H_2O)_4\{O_3PCH_2PO_3\}]$,[24] layered phases possessing structurally well-defined internal void spaces and coordination sites allowing the intercalation of alcohols by coordination of the substrate molecule to the vanadium sites of the V−P−O layer. We recently demonstrated that the chemistry of the $V-O-RPO_3^{2-}$ system can be dramatically expanded by the introduction of

⊗ Abstract published in *Advance ACS Abstracts,* July 15, 1995.

(1) (a) Syracuse University. (b) NEC Research Institute. (c) NSF-REU Fellow, Summer 1994, Syracuse University. (d) University of New Orleans.
(2) Zubieta, J. *Comments Inorg. Chem.* **1994**, *16*, 153 and references therein.
(3) Chen, Q.; Salta, J.; Zubieta, J. *Inorg. Chem.* **1993**, *32*, 4485.
(4) Bhardwaj, C.; Hu, H.; Clearfield, A. *Inorg. Chem.* **1993**, *32*, 4294 and references therein.
(5) Alberti, G.; Constantino, U.; Marmottini, F.; Vivani, R.; Zappelli, P. *Angew. Chem.* **1993**, *105*, 1396; *Angew. Chem., Int. Ed. Engl.* **1993**, *32*, 1357 and references therein.
(6) Alberti, G.; Constantino, U. In *Inclusion Compounds 5*; Atwood, J. L., Davis, J. E. D., MacNicol, C. D. D., Eds.; Oxford University Press: Oxford, U.K., 1991; Chapter 5.
(7) Burwell, D. A.; Thompson, M. E. *ACS Symp. Ser.* **1992**, *499*, 166.
(8) Clearfield, A.; Ortiz-Avila, C. Y. *ACS Symp. Ser.* **1992**, *499*, 178.
(9) Clearfield, A. *Inorganic Ion Exchange Materials*; CRC Press: Boca Raton, FL, 1982; p 1.
(10) Clearfield, A. In *Design of New Materials*; Cocke, D. L., Clearfield, A., Eds.; Plenum: New York, 1986.
(11) Rosenthal, G. L.; Caruso, J. *Inorg. Chem.* **1992**, *31*, 144.
(12) Zhang, Y.; Clearfield, A. *Inorg. Chem.* **1992**, *31*, 2821.
(13) Burwell, D. A.; Valentine, K. G.; Timmermans, J. H.; Thompson, M. E. J. *Am. Chem. Soc.* **1992**, *114*, 4144.
(14) Gao, G.; Mallouk, T. E. *Inorg. Chem.* **1991**, *30*, 1434.
(15) Wang, R.-C.; Zhang, Y.; Hu, H.; Frausto, R. R.; Clearfield, A. *Chem. Mater.* **1992**, *4*, 864.
(16) Lee, H.; Keply, T. J.; Hong, H.-G.; Akhter, S.; Mallouk, T. G. *J. Phys. Chem.* **1988**, *92*, 2597.
(17) Yang, H. C.; Aoki, K.; Hong, H.-G.; Sackett, D.; Arendt, M. F.; Yan, S.-L.; Bell, C. M.; Mallouk, T. E. *J. Am. Chem. Soc.* **1993**, *115*, 11855.
(18) Katz, H. E.; Wilson, W. L.; Scheller, G. *J. Am. Chem. Soc.* **1994**, *116*, 6636.
(19) Ungashe, S. B.; Wilson, W. L.; Katz, H. E.; Scheller, G. R.; Putrinski, T. M. *J. Am. Chem. Soc.* **1992**, *114*, 8717.
(20) Byrd, H.; Pike, J. K.; Talham, D. R. *J. Am. Chem. Soc.* **1994**, *116*, 7903.
(21) Johnson, J. W.; Jacobson, A. J.; Butler, W. M.; Rosenthal, S. E.; Brody, J. F.; Lewandowski, J. T. *J. Am. Chem. Soc.* **1989**, *111*, 381.
(22) Huan, G. H.; Jacobson, A. J.; Johnson, J. W.; Corcoran, E. W., Jr. *Chem. Mater.* **1990**, *2*, 2.
(23) Huan, G. H.; Johnson, J. W.; Jacobson, A. J.; Merola, J. S. *J. Solid State Chem.* **1990**, *89*, 220.
(24) Huan, G. H.; Jacobson, A. J.; Johnson, J. W.; Goshorn, D. P. *Chem. Mater.* **1992**, *4*, 661.

0020-1669/95/1334-4460$09.00/0

cationic templating reagents as structure-directing units. In this fashion, progressively more radical modifications of the layered structures of the V−O−RPO_3^{2-} phases $(EtNH_3)[(VO)_3(H_2O)(PhPO_3)_4]$,[25] $(Et_2NH_2)(Me_2NH_2)[(VO)_4(OH)_2(PhPO_3)_4]$,[26] and $(Et_4N)_2[(VO)_6(OH)_2(H_2O)_2(EtPO_3)_6]$[27] were effected by the introduction of appropriate templates. In the case of the oxovanadium diphosphonate system, V−O−$R'(PO_3)_2^{4-}$, "engineering" of the structure of the material could be accomplished both by introduction of different templates and by changes in the length and structure of diphosphonate tether R′, as we demonstrated in the isolation of 1-D, 2-D, and 3-D structural types, $[H_2N(C_2H_4)_2NH_2][(VO)(O_3PCH_2PO_3)]$, $[H_3NCH_2CH_2NH_3][(VO)(O_3PCH_2CH_2PO_3)]$, and $[H_3NCH_2CH_2NH_3][(VO)_4(OH)_2(H_2O)_2(O_3PCH_2CH_2CH_2PO_3)_2]\cdot 4H_2O$, respectively.[28]

Encouraged by these results, we have continued to develop the chemistry of the V−O−$R'(PO_3)_2^{4-}$ system by studying variations in reaction conditions, tether structures, and templates. The structural consequences of such variations are apparent in the title complexes $[H_2N(C_2H_4)NH_2][(VO)_2)O_3PCH_2CH_2CH_2PO_3)_2]$ (**1**) and $[(VO)(H_2O)\{O_3PCH_2NH(C_2H_4)_2NHCH_2PO_3\}]$ (**2**), both of which incorporate piperazine motifs, $-N(C_2H_4)_2N-$, but as an intercalated piperazinium cation in **1** and as both cation and the diphosphonate tether in **2**. The influence of reaction conditions is further evident in the "stair-step" structure adopted by **1** which contrasts with the 3-D structure of $[H_3NCH_2CH_2NH_3][(VO)_4(OH)_2(H_2O)_2(O_3PCH_2CH_2CH_2PO_3)_2]\cdot 4H_2O$, a material containing the same diphosphonate but a different templating reagent. While the structure of the V−P−O ribbons of **1** is directly related to the $\{(VO)_2(\mu_2\text{-}O_2P(O)Ph)_2\}$ motif of the prototypical $[(VO)(PhPO_3)(H_2O)]$, that of **2** is a defected form of the V−P−O plane of **1**, with alternate vanadium sites vacant. The structure of the fundamental building block of **1** is reflected in its magnetic properties, which may be compared to those observed for other members of the oxovanadium−organophosphonate class of materials, namely, the 1-D phase $[H_2N(CH_2CH_2)_2NH_2][(VO)(O_3PCH_2PO_3)]$ and the 2-D material $[H_3NCH_2CH_2NH_3][(VO)(O_3PCH_2CH_2PO_3)]$.

Experimental Section

Hydrothermal reactions were carried out in Parr acid digestion bombs with 23 mL poly(tetrafluoroethylene) liners or in borosilicate tubes with 15 mm outer diameter, 11 mm inner diameter, and length of 254 mm. Piperazine, propylenediphosphonic acid, and VCl_4 were purchased from Aldrich. The VCl_4 was carefully hydrolyzed to give a turquoise solution of "VO^{2+}", which was used as the vanadium(IV) source. The concentration of the solution was 1.47 M. Infrared spectra were obtained on a Perkin-Elmer 1600 Series FTIR spectrometer.

Synthesis of $[H_2N(C_2H_4)_2NH_2][(VO)_2(O_3PCH_2CH_2CH_2PO_3H)_2]$ (1). A mixture of VCl_4 (0.40 mL, 0.59 mmol), propylenediphosphonic acid (0.18 g, 0.88 mmol), piperazine (0.15 g, 1.74 mmol), and H_2O (10 mL, 44% fill volume) in the mole ratio 1:1.5:3:945 was heated at 200 °C for 96 h in a Parr bomb. After the mixture was cooled to room temperature, green rodlike crystals of **1** were collected in 65% yield, based on vanadium. IR (KBr pellet, cm^{-1}): 3431 (m), 3091 (m), 3025 (m), 2960 (m), 2718 (m), 2433 (m), 2367 (w), 1614 (m), 1460 (m), 1241 (m), 1203 (m), 1109 (s), 1071 (s), 1038 (s), 989 (m), 951 (m), 929 (sh), 824 (w), 753 (m), 709 (w), 594 (m), 523 (m), 485 (m). Anal. Calcd for $C_{10}H_{26}N_2O_{14}P_4V_2$: C, 19.2; H, 4.17; N, 4.49. Found: C, 18.9; H, 3.97; N, 4.63.

(25) Khan, M. I.; Lee, Y.-S.; O'Connor, C. J.; Haushalter, R. C.; Zubieta, J. *Inorg. Chem.* **1994**, *33*, 3855.
(26) Khan, M. I.; Lee, Y.-S.; O'Connor, C. J.; Haushalter, R. C.; Zubieta, J. *J. Am. Chem. Soc.* **1994**, *116*, 4525.
(27) Khan, M. I.; Lee, Y.-S.; O'Connor, C. J.; Haushalter, R. C.; Zubieta, J. *Chem. Mater.* **1994**, *6*, 721.
(28) Soghomonian, V.; Chen, Q.; Haushalter, R. C.; Zubieta, J. *Angew. Chem., Int. Ed. Engl.* **1995**, *34*, 223.

Table 1. Summary of Crystallographic Data for the Structures of $[H_2N(C_2H_4)_2NH_2][(VO)_2(O_3PCH_2CH_2CH_2PO_3H)_2]$ (**1**) and $[(VO)(H_2O)\{O_3PCH_2NH(C_2H_4)_2NHCH_2PO_3\}]$ (**2**)

	1	**2**
formula	$C_{10}H_{26}N_2O_{14}P_4V_2$	$C_6H_{12}N_2O_8P_2V$
fw	624.0	353.1
space group	$P\bar{1}$ (No. 2)	$P2_1/c$ (No. 14)
a, Å	6.244(1)	7.999(2)
b, Å	8.687(2)	8.009(2)
c, Å	11/156(2)	9.201(2)
α, deg	88.92(3)	
β, deg	74.63(3)	100.24(3)
γ, deg	74.32(3)	
V, Å^3	560.8(3)	580.1(3)
Z	1	2
D_{calc}, g cm^{-3}	1.842	2.021
μ, cm^{-1}	11.88	11.71
range of transm factors	0.92−1.03	0.84−0.92
T, K	294	253
radiation	Mo Kα (graphite monochromated, λ = 0.710 73 Å)	
no. of reflns used ($I_o \geq 3\sigma(I_o)$)	1663	1453
R^a	0.066	0.059
R_w^b	0.080	0.069

^{a} $R = \sum||F_o| - |F_c||/\sum|F_o|$. ^{b} $R_w = [\sum w(|F_o| - |F_c|)^2/\sum w(|F_o|)^2]^{1/2}$.

Table 2. Atomic Positional Parameters (×10^4) and Isotropic Thermal Parameters (Å^2 × 10^3) for **1**

	x	y	z	U(eq)^a
V(1)	2342(2)	8784(2)	6607(1)	13(1)
P(1)	2090(3)	11368(2)	4438(2)	14(1)
P(2)	1253(3)	5825(2)	8395(2)	17(1)
O(1)	−1553(10)	−143(7)	2314(5)	26(2)
O(2)	674(8)	1402(6)	3494(4)	16(2)
O(3)	−2664(8)	249(6)	5006(5)	18(2)
O(4)	4285(8)	1816(7)	3710(5)	22(2)
O(5)	−2696(9)	3267(7)	2576(5)	24(2)
O(6)	−2964(9)	5426(7)	1108(5)	28(2)
O(7)	712(9)	3155(6)	680(5)	22(2)
N(1)	4343(11)	10969(8)	1119(6)	24(2)
C(1)	407(13)	2872(10)	5646(8)	24(3)
C(2)	1767(13)	3562(10)	6373(7)	22(3)
C(3)	−42(15)	5297(10)	2514(8)	27(3)
C(4)	4261(15)	9294(10)	1169(8)	27(3)
C(5)	3806(15)	8804(11)	−1(8)	29(3)

^{a} Equivalent isotropic U defined as one-third of the trace of the orthogonalized U_{ij} tensor.

Synthesis of $[(VO)(H_2O)\{O_3PCH_2NH(C_2H_4)_2NHCH_2PO_3\}]$ (2). A mixture of VCl_4 (0.39 mL, 0.57 mmol), *N*,*N*′-piperazinebis(methylenephosphonic acid) (0.13 g, 0.47 mmol), and water (6 mL, 26% fill volume) in the mole ratio 1:0.8:570 was heated at 125 °C for 134 h in a borosilicate tube. After cooling of the mixture to room temperature, washing with water, and air-drying, compound **2** was isolated as lightly colored blue-green blockish crystals in 50% yield, based on vanadium. IR (KBr pellet, cm^{-1}): 3425 (m), 3010 (w), 2977 (m), 1451 (w), 1320 (w), 1216 (m), 1091 (vs), 1003 (s), 965 (s), 883 (w), 818 (m), 763 (m), 616 (w), 583 (w), 528 (m). Anal. Calcd for $C_6H_{16}N_2O_8P_2V$: C, 20.2; H, 4.48; N, 7.84. Found: C, 19.8; H, 4.57; N, 7.63.

X-ray Crystallographic Studies. The experimental X-ray data for the structures of **1** and **2** are summarized in Table 1; atomic coordinates are listed in Tables 2 and 3, and selected bond lengths and angles are presented in Tables 4 and 5.

Data were collected on a Rigaku AFC5S four-circle diffractometer. In the case of **2**, crystal stability was considerably improved by cooling to −20 °C. In neither case was significant crystal decomposition observed during the course of the data collection.

In both cases, data were corrected for Lorentz, polarization, and absorption effects in the usual fashion. Both structures were solved by Patterson techniques and refined by full-matrix least-squares methods using SHELXTL. In both cases, refinement proceeded routinely, and

Table 3. Atomic Positional Parameters ($\times 10^4$) and Isotropic Thermal Parameters ($Å^2 \times 10^3$) for **2**

	x	y	z	U(eq)[a]
V(1)	−554(1)	−24(2)	4894(1)	12(1)
P(1)	1166(1)	−1810(1)	2211(1)	13(1)
O(1)	253(4)	−2765(4)	880(3)	25(1)
O(2)	−100(3)	−1037(3)	3055(3)	21(1)
O(3)	2592(4)	−2759(5)	3137(4)	37(1)
O(4)	−2553(4)	−139(5)	4675(4)	37(1)
N(1)	6662(4)	300(4)	−464(3)	15(1)
C(1)	2083(5)	32(4)	1463(4)	17(1)
C(2)	3764(5)	1310(5)	−210(5)	23(1)
C(3)	4964(5)	−1044(5)	1259(4)	24(1)

[a] Equivalent isotropic U defined as one-third of the trace of the orthogonalized U_{ij} tensor.

Table 4. Selected Bond Lengths (Å) and Angles (deg) for **1**

V(1)−O(1A)	1.585(6)	V(1)−O(2B)	1.965(6)
V(1)−O(3A)	1.957(5)	V(1)−O(4B)	1.963(5)
V(1)−O(5A)	1.971(6)	P(1)−O(2A)	1.540(6)
P(1)−O(3A)	1.516(6)	P(1)−O(4A)	1.541(6)
P(1)−C(1A)	1.789(8)	P(2)−O(5A)	1.506(6)
P(2)−O(6A)	1.577(6)	P(2)−O(7A)	1.518(5)
P(2)−C(3A)	1.769(11)	O(1)−V(1A)	1.585(6)
O(2)−V(1A)	1.965(6)	O(2)−P(1A)	1.540(6)
O(3)−V(1A)	1.957(5)	O(3)−P(1B)	1.516(6)
O(4)−V(1B)	1.963(5)	O(4)−P(1A)	1.541(6)
O(5)−V(1A)	1.971(6)	O(5)−P(2A)	1.506(6)
O(6)−P(2A)	1.577(6)	O(7)−P(2A)	1.518(5)
N(1)−C(4)	1.469(12)	N(1)−C(5A)	1.510(10)
C(1)−C(2)	1.548(14)	C(1)−P(1A)	1.789(8)
C(2)−C(3A)	1.564(10)	C(3)−P(2A)	1.769(11)
C(3)−C(2A)	1.564(10)	C(4)−C(5)	1.500(14)
C(5)−N(1A)	1.510(10)	C(4)−C(5)	1.500(14)
O(1A)−V(1)−O(2B)	100.6(3)	O(1A)−V(1)−O(3A)	109.6(3)
O(2B)−V(1)−O(3A)	87.8(2)	O(1A)−V(1)−O(4B)	101.8(3)
O(2B)−V(1)−O(4B)	157.1(2)	O(3A)−V(1)−O(4B)	89.1(2)
O(1A)−V(1)−O(5A)	106.3(3)	O(2B)−V(1)−O(5A)	87.0(2)
O(3A)−V(1)−O(5A)	144.0(2)	O(4B)−V(1)−O(5A)	82.3(2)
O(2A)−P(1)−O(3A)	112.4(3)	O(2A)−P(1)−O(4A)	105.3(3)
O(3A)−P(1)−O(4A)	111.8(3)	O(2A)−P(1)−C(1A)	107.3(3)
O(3A)−P(1)−C(1A)	109.7(3)	O(4A)−P(1)−C(1A)	110.1(4)
O(5A)−P(2)−O(6A)	106.2(3)	O(5A)−P(2)−O(7A)	115.2(3)
O(6A)−P(2)−O(7A)	109.5(3)	O(5A)−P(2)−C(3A)	111.8(4)
O(6A)−P(2)−C(3A)	106.5(4)	O(7A)−P(2)−C(3A)	107.3(4)
V(1A)−O(2)−P(1A)	141.2(3)	V(1A)−O(3)−P(1B)	140.8(3)
V(1B)−O(4)−P(1A)	143.2(4)	V(1A)−O(5)−P(2A)	139.9(3)
C(4)−N(1)−C(5A)	111.3(6)	C(2)−C(1)−P(1A)	116.3(5)
C(1)−C(2)−C(3A)	109.7(7)	P(2A)−C(3)−C(2A)	116.2(6)
N(1)−C(4)−C(5)	109.2(7)	C(4)−C(5)−N(1A)	109.8(8)

no anomalies in temperature factors or excursions of electron density in the final Fourier maps were observed.

In the case of **2**, the vanadium site is disordered about the crystallographic center of symmetry, so as to orient on either face of the plane generated by the four oxygen donors of the diphosphonate ligands and along the {O=V−OH_2} axis.

Magnetic Measurements. The magnetic susceptibility data were recorded on polycrystalline samples over the 2−300 K temperature region using a Quantum Design MPMS-5S SQUID susceptometer. Measurement and calibration techniques have been reported elsewhere.[29] The temperature-dependent magnetic data were measured at a magnetic field of 1000 G.

Results and Discussion

Syntheses, Infrared Spectra, and Structural Descriptions. Hydrothermal synthesis has been demonstrated to provide a low-temperature pathway to metastable structures utilizing inorganic and organic molecular units of a desired geometry and allowing the introduction of a variety of inorganic and/or organic cations as templates for the organization of the networks of oxovanadium polyhedra and phosphorus tetrahedra.[25−28,30] However, it has become clear that the identity of the product isolated is critically dependent on reaction conditions and that the parameter space associated with the hydrothermal technique is vast, with factors such as temperature, stoichiometries, pH, fill volume, surface nucleation, nature of the oxometal source, and templating reagents contributing to the chemistry. The structural chemistry of the V−O−PO_4^{3-} system has been demonstrated to be extensive,[31] and our continuing investigations suggest that a correspondingly rich chemistry will emerge for the V−O−RPO_3^{2-} and V−O−R′$(PO_3)_2^{4-}$ systems. The observations that reactions of oxovanadium sources with the same diphosphonate in the presence of different templates or with diphosphonates with different backbones result in novel phases are thus not unexpected.

Table 5. Selected Bond Lengths (Å) and Angles (deg) for **2**

V(1)−O(2)	1.967(3)	V(1)−O(4)	1.578(4)
V(1)−O(1A)	1.974(3)	V(1)−O(1B)	2.041(3)
V(1)−O(2A)	2.051(3)	P(1)−O(1)	1.517(3)
P(1)−O(2)	1.514(3)	P(1)−O(3)	1.503(3)
P(1)−C(1)	1.835(4)	N(1)−C(1A)	1.501(5)
N(1)−C(2A)	1.495(5)	N(1)−C(3A)	1.498(5)
C(1)−N(1A)	1.501(5)	C(2)−N(1A)	1.495(5)
C(2)−C(3A)	1.538(6)	C(3)−N(1A)	1.498(5)
C(3)−C(2A)	1.538(6)	C(3)−N(1A)	1.498(5)
O(2)−V(1)−O(4)	101.8(2)	O(2)−V(1)−O(1A)	90.8(1)
O(4)−V(1)−O(1A)	101.1(2)	O(2)−V(1)−O(1B)	86.1(1)
O(4)−V(1)−O(1B)	103.9(2)	O(1A)−V(1)−O(1B)	154.9(1)
O(2)−V(1)−O(2A)	155.0(1)	O(4)−V(1)−O(2A)	103.2(2)
O(1A)−V(1)−O(2A)	85.7(1)	O(1B)−V(1)−O(2A)	86.7(1)
O(1)−P(1)−O(2)	110.5(2)	O(1)−P(1)−O(3)	114.3(2)
O(2)−P(1)−O(3)	115.2(2)	O(1)−P(1)−C(1)	105.6(2)
O(2)−P(1)−C(1)	102.2(2)	O(3)−P(1)−C(1)	107.8(2)
P(1)−O(1)−V(1C)	149.9(2)	V(1)−O(2)−P(1)	148.5(2)
C(1A)−N(1)−C(2A)	109.1(3)	C(1A)−N(1)−C(3A)	112.9(3)
C(2A)−N(1)−C(3A)	107.7(3)	P(1)−C(1)−N(1A)	116.3(2)
N(1A)−C(2)−C(3A)	111.4(3)	N(1A)−C(3)−C(2A)	111.2(3)

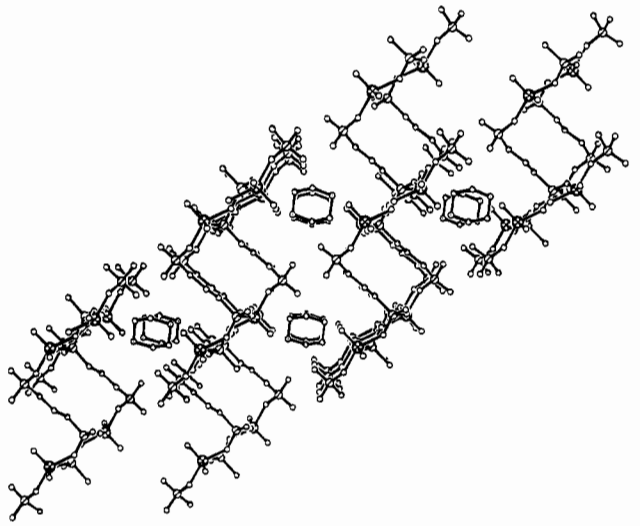

Figure 1. View of the structure of **1** parallel to the crystallographic a axis, showing the stair-step layer motif consisting of infinite ribbons four polyhedra in width and the locations of the $[H_2N(C_2H_4)_2NH_2]^{2+}$ cations in the interlarmellar cavities. Vanadium atoms are cross-hatched; phosphorus, shaded bottom left to top right; oxygen, open circles; carbon, small lightly shaded circles.

(29) O'Connor, C. J. *Prog. Inorg. Chem.* **1982**, *29*, 203.

(30) Soghomonian, V.; Chen, Q.; Haushalter, R. C.; Zubieta, J.; O'Connor, C. J. *Science* **1993**, *259*, 1596.

(31) Soghomonian, V.; Haushalter, R. C.; Chen, Q.; Zubieta, J. *Inorg. Chem.* **1994**, *33*, 1700 and references therein.

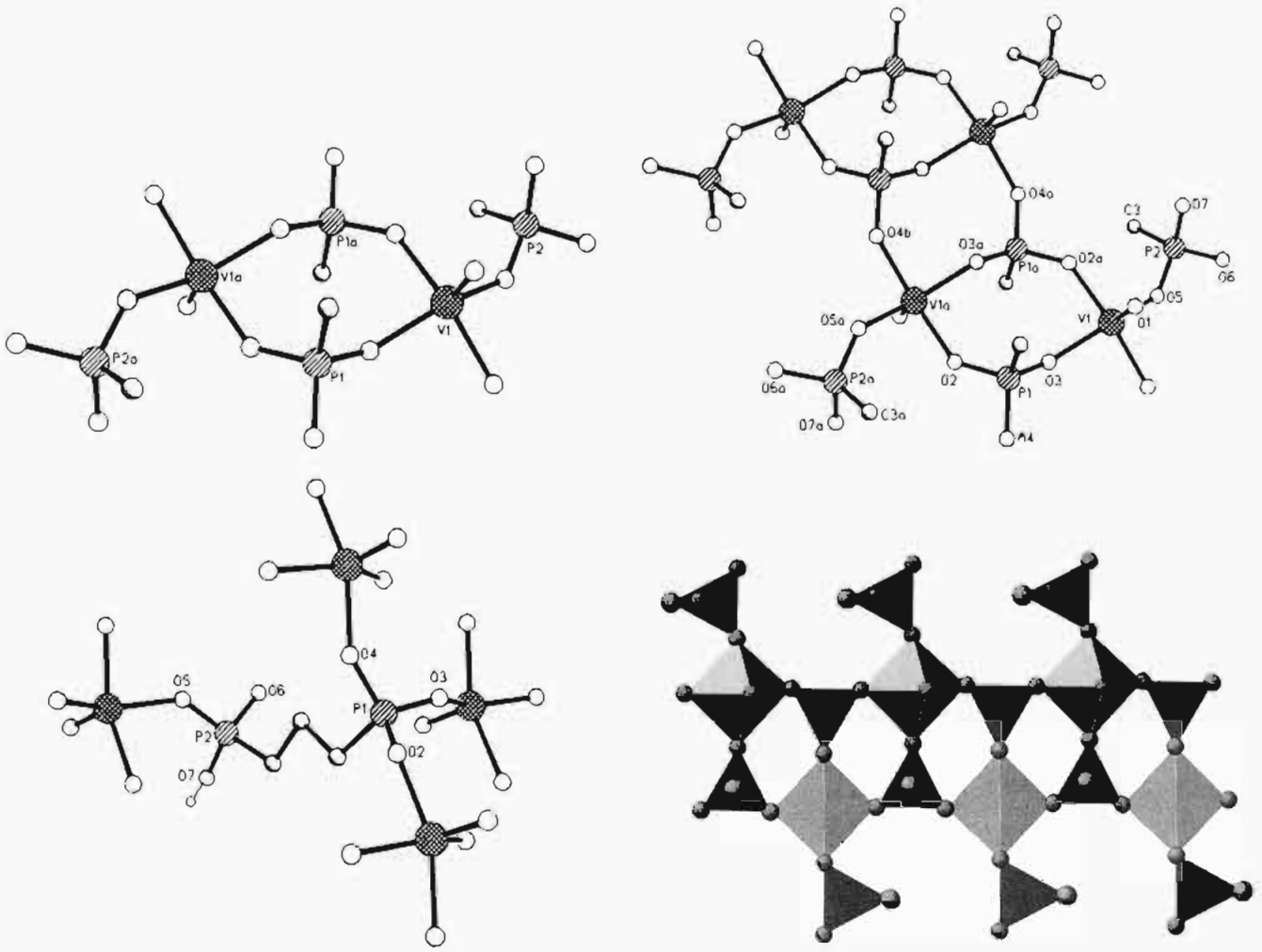

Figure 2. (a) Top left: View of the $\{V_2P_2O_4\}$ rings which provide the building block of the V−P−O layer of **1**. (b) Bottom left: Ligand coordination adopted by the diphosphonate group in **1**. (c) Top right: View of the V−P−O plane of $[VO(H_2O)(O_3PPh)]$. (d) Bottom right: Polyhedral representation of the V−P−O ribbons of **1**.

The syntheses of **1** and **2** used carefully hydrolyzed solutions of VCl_4 as the source of hydrated VO^{2+} species. The oxidation state of the vanadium as V(IV) was confirmed by redox titration.[32] The use of the V(IV) precursor appears to suppress the formation of mixed-valence species, such as $[V_{15}O_{36}X]^{6-}$,[33] and $[V_{10}O_{26}]^{4-}$.[34]

The reaction of a mixture of VCl_4, propylenediphosphonic acid, piperazine, and H_2O in the mole ratio 1:1.5:3:945 at 200 °C for 96 h yields green rods of $[H_2N(C_2H_4)_2NH_2][(VO)_2(O_3PCH_2CH_2CH_2PO_3H)_2]$ (**1**) in 65% yield. The infrared spectrum of **1** exhibits two strong bands at 1071 and 1038 cm^{-1} assigned to the asymmetric and symmetric $-PO_3^{2-}$ stretching modes, respectively, and a sharp band at 967 cm^{-1} assigned to $\nu(V{=}O)$.

The overall structure of **1** may be described as parallel V/P/O ribbons linked through the propylene backbone of the diphosphonate ligands, as shown in Figure 1. The vanadium sites exhibit square pyramidal geometry defined by coordination to four oxygen donors from each of four adjacent diphosphonate ligands and to the terminal oxo ligand (Figure 2a). The V(IV) oxidation state is confirmed by the bond lengths listed in Table 3 and the valence sums associated with these values.[35] The coordination mode adopted by the diphosphonate ligand is unusual: the P(1) site employs all three oxygen atoms to bond to three adjacent vanadium sites of a single V−P−O ribbon while the P(2) site bonds through a single oxygen donor to a vanadium center of an adjacent ribbon (Figure 2b). Two oxygen atoms of the P(2) site are pendant, O(6) as a terminal {P=O} unit and O(7) as a protonated site {P−OH}. The resultant bonding within the V−P−O ribbons consists of corner-sharing vanadium square pyramids and phosphorus tetrahedra.

The repeating structural motif within the layers is the binuclear phosphonate-bridged eight-membered ring $\{(VO)_2(\mu_2\text{-}O_2P(O)Ph)_2\}$, a characteristic building block of both V−O−PO_4^{3-} and V−O−RPO_3^{2-} systems. Although the prototypical $[VO(PhPO_3)(H_2O)]$ structure also exhibits the $\{(VO)_2(\mu_2\text{-}O_2P(O)Ph)_2\}$ unit as a structural motif, the corner-sharing interaction between vanadium sites to produce infinite {V=O···V=O} chains generates twelve-membered $\{V_4P_2O_6\}$ rings and six-membered $\{V_2PO_3\}$ rings as well (Figure 2c). In the case of **1**, the ribbon structure is generated by the fusing of the $\{V_2O_2O_4\}$ rings through the O(4) sites of adjacent P(1) centers to produce the chain illustrated in Figure 2d.

The presence of the P(2) sites as $\{RPO_3H\}^-$ tetrahedra with pendant {P=O} and {P−OH} groups serves to terminate the corner-sharing motif of vanadium square pyramids and phosphorus tetrahedra, resulting in a ribbon structure for the V−P−O layers, which are four polyhedra in width from edge-defining P(2) group to edge-defining P(2) group and are infinitely long

(32) Hentz, F. C., Jr.; Long, G. G. *J. Chem. Educ.* **1978**, *55*, 55.
(33) Müller, A.; Penk, M.; Rohlfing, R.; Krickemeyer, E.; Döring, J. *Angew. Chem., Int. Ed. Engl.* **1990**, *29*, 926.
(34) Bino, A.; Cohen, S.; Heitner-Wiguin, C. *Inorg. Chem.* **1982**, *21*, 429.
(35) Brown, I. D. In *Structure and Bonding in Crystals*; O'Keefe, M., Navrotsky, A., Eds.; Academic Press: New York, 1981; Vol. 11, pp 1−30.

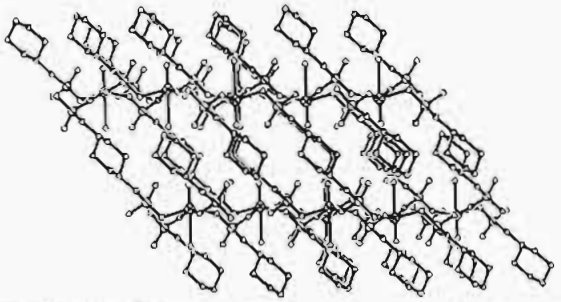

Figure 3. View along the [010] crystallographic direction of the structure of **2**, illustrating the "pillaring" of the inorganic V−P−O layers by the $\{-CH_2NH(C_2H_4)_2NHCH_2-\}$ backbones of the diphosphophonate ligands.

parallel to *b*. The diphosphonate groups serve to interconnect each ribbon to the two adjacent ribbons in such a fashion so as to generate a stair-step layer motif, reminiscent of that recently reported for $K_2[V_3O_2(H_2O)_2(PO_4)(HPO_4)(H_2PO_4)]$.[36] The $\{RPO_3H\}^-$ units of P(2) at the edges of the ribbons serve to interconnect the adjacent ribbons via hydrogen bonding with distances of 2.53 Å between O(7) of the P(2) units of one staircase and O(6) of the adjacent staircase.

The stacking and interleaving of the step layers produce cavities between the layers occupied by the piperazinium cations. The vanadyl oxygens and the pendant {P=O} and {P−OH} groups of the P(2) sites project into this cavity and define the cation environment. The most significant H-bonding interactions appear to be between the $\{-NH_2^+\}$ groups and the vanadyl oxo units and between the $\{NH_2^+\}$ groups and the phosphonate pendant O(7) sites, with N···O distances of 3.11 and 2.69 Å, respectively.

When a mixture of VCl_4, *N,N'*-piperazinebis(methylenephosphonic acid), and H_2O in the mole ratio 1:0.8:570 is heated at 125 °C for 134 h, $[(VO)(H_2O)\{O_3PCH_2NH(C_2H_4)_2NHCH_2PO_3\}]$ (**2**) is isolated as blue-green blocks in 50% yield. Since the pH of the reaction solution is *ca.* 5, it is not surprising that the piperazine tether has been protonated at the nitrogen sites to yield a bridging $\{O_3PCH_2NH(C_2H_4)_2NHCH_2PO_3\}^{2-}$ unit. The infrared spectrum of **2** is characterized by strong bands at 1091 and 1003 cm^{-1} associated with PO_3^{2-} stretching modes and a feature at 965 cm^{-1} assigned to ν(V=O).

The structure of **2**, as shown in Figure 3, consists of corner-sharing vanadium octahedra and phosphorus tetrahedra fused to generate inorganic V−P−O layers covalently joined by the $\{-CH_2NH(C_2H_4)_2NHCH_2-\}^{2+}$ backbones of the organodiphosphonate ligands. The resultant structure may be described as inorganic V−P−O layers "pillared" by intervening cationic organic layers or, alternatively, as a 3-D V−P−O−C covalently linked framework. The vanadium site exhibits octahedral geometry defined by four oxygen donors from each of four phosphonate groups in an equatorial arrangement, with a terminal oxo ligand and the oxygen donor of an aquo ligand occupying the axial positions. Each organodiphosphonate group coordinates through two oxygen donors of either $\{-PO_3\}^{2-}$ terminus, leaving one {P=O} unit pendant at each phosphorus site (Figure 4b).

The vanadium octahedra and phosphorus tetrahedra are linked in a corner-sharing mode to produce sixteen-membered $\{V_4P_4O_8\}$ rings (Figure 4a) which fuse so as to generate the layer structure illustrated in Figure 4b. It is noteworthy that the layer structures of **1** and **2** are quite distinct. However, the repeating eight-membered ring $\{V_2P_2O_4\}$ unit of **1** may be produced in **2** by addition of a vanadium site at the centroid of each $\{V_4P_4O_8\}$ ring, suggesting that the layer structure of **2** may be viewed as a defected form of that observed for **1** or, alternatively, as a defected $[VO(PO_4)]$ layer with half the V sites vacant. The structural motifs are thus a direct reflection of the V:P ratios of **1** and **2**, that is, 1:2 and 1:1, respectively.

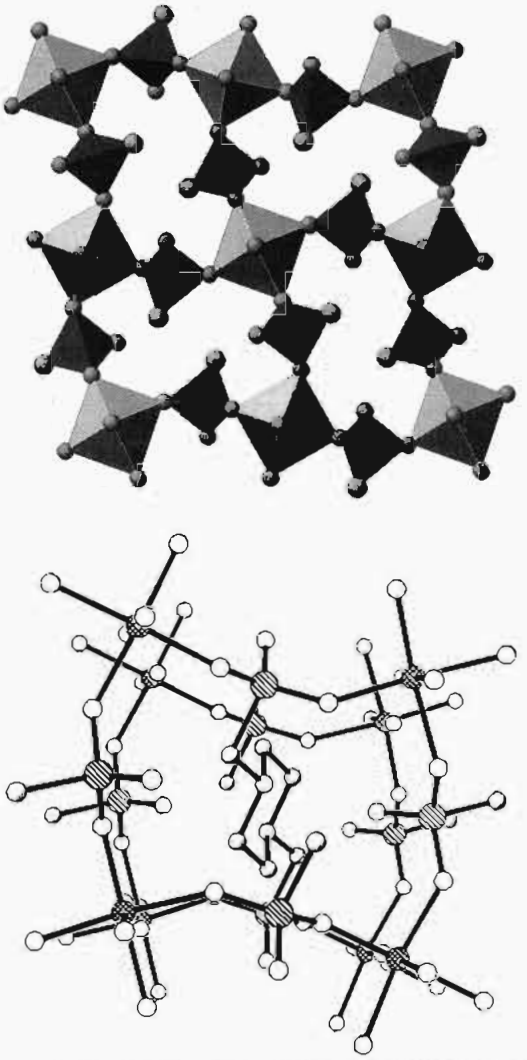

Figure 4. (a) Top: Polyhedral representation of the V−P−O layers of **2**, showing the $\{V_4P_4O_8\}$ rings which provide the repeating structural building block for the layer. (b) Bottom: View of the environment of one organodiphosphonate group, bridging adjacent V−P−O layers. The organic tether is located in the interlamellar region and aligned with the cavities of adjacent layers produced by the sixteen-membered ring motifs.

The organic backbones of the diphosphonate ligands project from either surface of the V/P/O planes, to produce a motif of alternating inorganic and organic layers, reminiscent of the structures of $[VO(H_2O)(PhPO_3)]$, $(EtNH_3)[(VO)_3(H_2O)(PhPO_3)_4]$,[25] and $(Et_4N)_2[(VO)_6(OH)_2(H_2O)_2(EtPO_3)_6]$.[27] The geometric requirements of the $-CH_2N(C_2H_4)_2NCH_2-$ backbone of **2** produce an unusual stacking of the V−P−O layers. Other examples of "pillared" oxovanadium diphosphonates, $[H_2N(C_2H_4)_2NH_2][(VO)_2(O_3PCH_2CH_2CH_2PO_3H)_2]$ (**1**) and $[H_3NCH_2CH_2NH_3][(VO)_4(OH)_2(H_2O)_2(O_3PCH_2CH_2CH_2PO_3)_2]\cdot 2H_2O$,[28] exhibit organic tethers which project at nearly right angles from the V−P−O planes, such that the V−P−O layer separation reflects the tether length directly. In contrast, the C(1)···C(1A) vector of the ligand backbone of **2** makes an angle of approximately 60° with the V−P−O layers. Consequently, the interlayer separation of 8.00 Å is *ca.* 1.00 Å shorter than the

(36) Haushalter, R. C.; Wang, Z.; Thompson, M. E.; Zubieta, J.; O'Connor, C. J. *Inorg. Chem.* **1993**, *32*, 3966.

optimal value produced by rotating the pendant {P=O} groups into the V−P−O planes and aligning the C(1)···C(1A) vectors perpendicular to the V−P−O planes. The layer repeat of 8.00 Å in **2** may be compared to values of 11.156 Å in **1** and 15.037 Å in $[(VO)_2(H_2O)_4\{(O_3P)_2CH_2\}]$.

Since the nitrogen centers of the ligand tethers are protonated in **2**, the V−P−O framework is negatively charged. Similarly, the oxovanadium diphosphonates **1**, **2**, $[H_2N(C_2H_4)_2NH_2][VO(O_3PCH_2PO_3)]$, $[H_3NCH_2CH_2NH_3][(VO)(O_3PCH_2CH_2PO_3)]$, and $[H_3NCH_2CH_2NH_3][(VO)_4(OH)_2(H_2O)_2(O_3PCH_2CH_2CH_2CH_2PO_3)_2]\cdot 4H_2O$[28] possess anionic V−P−O networks, while the compound $[(VO)_2\{(O_3P)_2CH_2\}_2(H_2O)_4]$[24] provides an unusual example of a diphosphonate with a neutral framework. However, the $V-O-R'(PO_3)_2^{4-}$ system exhibits considerable structural diversity, both within the inorganic V−P−O networks and with respect to the tether locations. Thus, phase **2** and $[(VO)_2\{(O_3P)_2CH_2\}_2(H_2O)_4]$ exhibit isolated $\{VO_6\}$ octahedra, that is, no {V−O−V} linkages, while phase **1** and $[H_3NCH_2CH_2NH_3][(VO)(O_3PCH_2CH_2PO_3)]$ possess isolated square pyramidal vanadium sites and $[H_3NCH_2CH_2NH_3][(VO)_4(OH)_2(H_2O)_2(O_3PCH_2CH_2CH_2PO_3)_2]\cdot 4H_2O$ exhibits both octahedral and square pyramidal sites and unique $\{V_2O_2(OH)\}$ binuclear units. While the organic backbones of the organodiphosphonate ligands of $[(VO)_2(H_2O)_4\{(O_3P)_2CH_2\}_2]$ and $[H_3NCH_2CH_2NH_3][(VO)(O_3PCH_2CH_2PO_3)]$ form part of the V/P/O/C 2-D networks of the layers (that is, both $(-PO_3)^{2-}$ termini of each ligand coordinate to vanadium sites of the same V−P−O layer), phases **1** and **2** and $[H_3NCH_2CH_2NH_3][(VO)_4(OH)_2(H_2O)_2(O_3PCH_2CH_2CH_2PO_3)_2]\cdot 4H_2O$ exhibit V−P−O layers "pillared" by the organic backbones of the ligands, such that the $(-PO_3)^{n-}$ groups of a given organodiphosphonate bond to adjacent V−P−O layers. It is also noteworthy that while phase **2** and $[(VO)_2(H_2O)_4\{(O_3P)_2CH_2\}_2]$ exhibit neutral networks, the remaining examples of oxovanadium diphosphonate phases require cationic templates to balance the negative charge of V−P−O networks. The chemistry of the oxovanadium−organophosphonate system remains insufficiently developed to predict the structure or the charge of the V−P−O framework based on the identity of the template or the tether linking the phosphonate units.

Magnetism. The magnetic properties of the "stair-step" compound **1** have been studied and compared to those of the 1-D and 2-D V−O−organophosphonato phases $[H_2N(C_2H_4)_2NH_2][(VO)(O_3PCH_2PO_3)]$ and $[H_3NCH_2CH_2NH_3][(VO)(O_3PCH_2CH_2PO_3)]$, respectively.

The high-temperature magnetic susceptibility data for the three V−O−organodiphosphonato phases exhibit Curie−Weiss paramagnetism:

$$\chi = C/(T - \Theta) = Ng^2\mu_B{}^2S(S+1)/[3k(T - \Theta)] \quad (1)$$

The high-temperature magnetic data were fit to the Curie−Weiss law. The 1-D material $[H_2N(C_2H_4)_2NH_2][(VO)(O_3PCH_2PO_3)]$ gave $C = 0.398$ emu K/mol, $\Theta = 0.4$ K, and TIP = 0.0 emu/mol. The 2-D layered compound $[H_3NCH_2CH_2NH_3][(VO)(O_3PCH_2CH_2PO_3)]$ was fit to $C = 0.485$ emu K/mol, $\Theta = -35$ K, and TIP = 0.0024 emu/mol, while the "stair-step" $[H_2N(C_2H_4)_2NH_2][(VO)_2(O_3PCH_2CH_2CH_2PO_3H)_2]$ (**1**) gave $C = 0.653$ emu K/mol, $\Theta = -83$ K, and TIP = 0.00024 emu/mol.

The electron structure of the three compounds corresponds to vanadium(IV) in the $3d^1$ electronic configuration. The 1-D material $[H_2N(C_2H_4)_2NH_2][(VO)(O_3PCH_2PO_3)]$ exhibits Curie−Weiss dependence over the entire temperature range and a very small Weiss constant. (Figure 5a). The V(IV) electron configuration gives a g value for this compound of 2.05.

In contrast, the 2-D materials $[H_3NC_2H_4NH_3][(VO)(O_3PCH_2CH_2PO_3)]$ and $[H_2N(C_2H_4)_2NH_2][(VO)_2(O_3PCH_2CH_2CH_2PO_3H)]$ (**1**) each exhibit a maximum in the temperature-dependent magnetic susceptibility The magnetic exchange that is expected in vanadium(IV) with a 2-D free ion ground term, d^1 electron structure, and spin $S = {}^1/_2$ is the isotropic Heisenberg spin Hamiltonian.

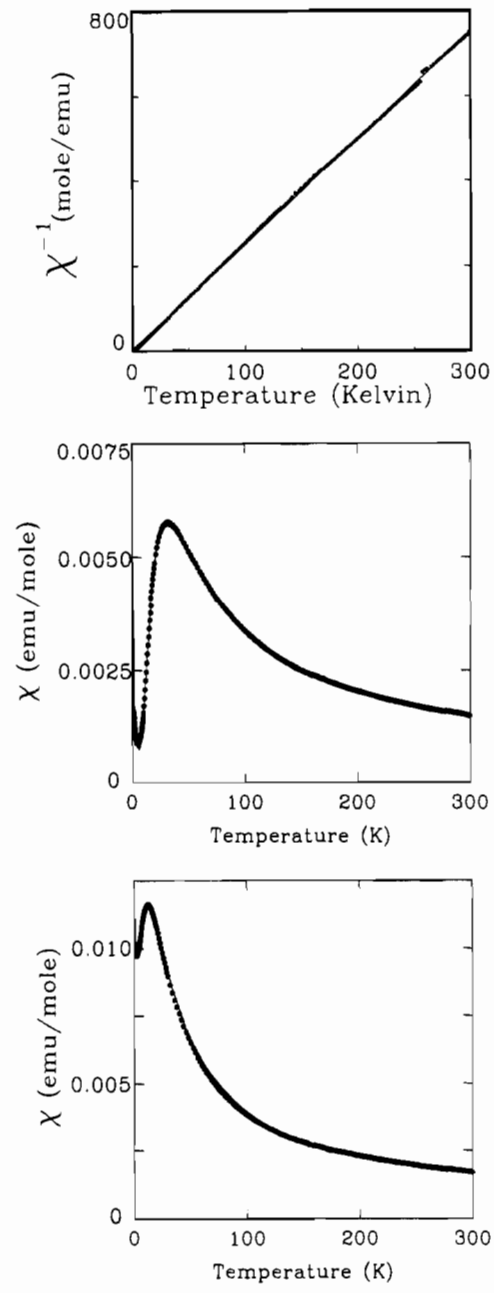

Figure 5. (a) Top: Inverse magnetic susceptibility of $[H_2N(C_2H_4)_2NH_2][(VO)(O_3PCH_2PO_3)]$ plotted as a function of temperature over the 1.7−300 K temperature region. The line drawn through the data is the fit to the Curie−Weiss model as described in the text. (b) Middle: Magnetic susceptibility of $[H_2N(C_2H_4)_2NH_2][(VO)_2(O_3PCH_2CH_2PO_3H)_2]$ plotted as a function of temperature over the 1.7−300 K temperature region. The curve drawn through the data is the fit to the binuclear exchange model as described in the text. (c) Bottom: Magnetic susceptibility of $[H_3NCH_2CH_2NH_3][(VO)(O_3PCH_2CH_2PO_3)]$ plotted as a function of temperature over the 1.7−300 K temperature region. The curve drawn through the data is the fit to the 1-D linear-chain model as described in the text.

$$\chi = -2JS_1\cdot S_2 \quad (2)$$

Compound **1** may be analyzed as a binuclear compound. The effect of the spin Hamiltonian on the behavior of a pair of

interacting electrons can be expressed as follows:

$$\chi = (Ng^2\mu_B{}^2/kT)e^{2J/kT}/(1 + 3e^{2J/kT}) \quad (3)$$

where a negative J denotes a ground state singlet, the susceptibility is calculated per V(IV) atom, and all of the parameters have their usual meaning.

The magnetic susceptibility data for **1** were analyzed with this equation, and a least-squares fit of eq 3 yields the parameters $g = 1.997$, $J/k = -25$ K; an additional term to correct for a temperature-independent paramagnetism was required as TIP = 0.000 28 emu/mol. The data were also corrected for a 1.2% paramagnetic (monomeric) impurity. The result of this fit is illustrated in Figure 5b, where magnetic susceptibility is plotted as a function of temperature and the smooth curve is the theoretical calculation. The layered material $[H_3NCH_2CH_2NH_3][(VO)(O_3PCH_2CH_2PO_3)]$ also exhibits a maximum in the temperature-dependent magnetic susceptibility. This material may be analyzed as a 1-D linear-chain compound using the numerical calculation for the 1-D $S = {}^1/_2$ system described by Bonner and Fisher.[37] In order to successfully analyze the data, we must correct the magnetic data for secondary magnetic exchange interactions using the molecular exchange field. The equation that describes the effect of a molecular exchange field on the magnetic susceptibility is

$$\chi = \chi'/\{1 - (zJ'/Ng^2\mu_B{}^2)\chi'\} + \text{TIP} \quad (4)$$

where χ' is the magnetic susceptibility of the material in the absence of the exchange field (eq 2) and χ is the molecular exchange field influenced magnetic susceptibility that is actually measured. The exchange field coupling parameter is zJ', where z is the number of exchange-coupled neighbors. The addition of the molecular field exchange correction resulted in a substantial improvement of the fit to the data. The temperature dependence of the magnetic susceptibility was determined using the Bonner–Fisher calculation corrected by eq 4 and gave the following fitted parameters: $g = 2.07$, $J/k = -10.3$ K, $zJ'/k = -2.7$ K, TIP = 0.000 34 emu/mol. The data were also corrected for the presence of a 0.6% paramagnetic (monomeric) impurity. The large value of zJ' indicates that all of the fitted parameters should be viewed with caution. Nevertheless the goodness of the fit indicates the primary coupling parameter $J/k = -10.3$ K is a good estimate of the strength of the exchange in this compound.

(37) Bonner, C. J.; Fisher, M. E. *Phys. Rev.* **1964**, *135*, A640.

Conclusions

The isolation of compounds **1** and **2** illustrates the power of hydrothermal synthesis in the preparation from molecular precursors of metastable phases not accessible through conventional high-temperature solid state techniques. The structures of these compounds when compared to those of other examples of the oxovanadium–organodiphosphonate system previously reported illustrate the structural versatility of the system and suggest that some primitive control of structural characteristics may be possible. While "designed" synthesis in the sense of predictability of product composition has yet to be achieved, the manipulation of hydrothermal reaction parameters, organic spacers in the tethers, and suitable templates allows the modification of interlayer spacings in 2-D structures, some control of the dimensionality of the solid phase, and the isolation of a range of phase compositions possessing unusual structural variability. Modifications of tether lengths, bulk, electronic properties, and functional groups should allow for the preparation of solids with specific interlayer spacings or well-defined void regions to give tailored microporosities[6,38] and of materials with tunable optical or electronic properties. The range of magnetic properties observed for the oxovanadium–organophosphonate class of materials appears to match the structural diversity. As the number of examples of this class expands, magneto–structural correlations should also evolve.

Acknowledgment. The work at Syracuse University was supported by NSF Grant CHE9318824. R.D. thanks the NSF-REU Program for Summer support.

Supporting Information Available: Tables of structure determination details, anisotropic temperature factors, and calculated hydrogen atom positions for **1** and **2** (8 pages). Ordering information is given on any current masthead page.

IC9501327

(38) Alper, J. *Chem. Ind.* **1986**, 335.